Journal of Solid Mechanics Vol. 11, No. 1 (2019) pp. 181-200
DOI: 10.22034/JSM.2019.664228

Study of the Effect of an Open Transverse Crack on the Vibratory Behavior of Rotors Using the *h-p* Version of the Finite Element Method

F. Ahmed *, H. Abdelhamid, B. Brahim, S. Ahmed

IS2M Laboratory, Faculty of Technology, University of Tlemcen, Algeria

Received 5 December 2018; accepted 5 February 2019

ABSTRACT

In this paper, we use the hybrid h-p version of the finite element method to study the effect of an open transverse crack on the vibratory behavior of rotors, the one-dimensional finite element Euler-Bernoulli beam is used for modeling the rotor, the shape functions used are the Hermite cubic functions coupled to the special Legendre polynomials of Rodrigues. The global matrices of the equation of motion of the cracked rotor are derived by the application of the Lagrange equation taking into account the local variation in the shaft's stiffness due to the presence of the crack, and the stiffness of the cracked element of the shaft are determined using the time-varying stiffness method. Numerical results generated by a program developed in MATLAB show the rapidity of the convergence of the h-p version of FEM compared to the classical version, after the validation of our results with theoretical and experimental results and other obtained with the simulator ANSYS Workbench, a parametric study was provided to show the influence of the depth and position of the crack on the vibratory behavior of a symmetrical and asymmetrical rotor.

Keywords: Rotor, Open transverse crack, *h-p* version of FEM, Time-varying stiffness.

1 INTRODUCTION

THE finite element method is the most method used for the numerical modeling of mechanical structures, the classical version calling *h* of this method was the first to be developed [1,2], it consists of discretizing the structure into a set of finite elements and its convergence is obtained by the increasing of the number of elements of the mesh with a fixed polynomials degree. During the 1970s, the hierarchical version calling p was developed [3-5], in this method we do not discretize the structure like the classical version, and the convergence of this method is obtained by the increasing of the degree of polynomials. The combination of these two versions leads to the hybrid *h-p* version of the FEM [6-8], the convergence of this method is obtained by the increasing of the number of elements of the mesh and by the increasing of the degree of polynomials of each element, and the rapidity of the convergence makes the efficiency of this method. The *h-p* version of the FEM is more used in the field of simple

*Corresponding author. Tel.: +21 3669571530.
E-mail address: fellah-gim@hotmail.fr (F.Ahmed).

structures such as beams, plates and shells, in the field of rotor vibration; this version is less used, we can mention the work of Boukhalfa, A, and Hadjoui, A [9], and the work of Saimi, A and Hadjoui, A [10]. The cracks are classified among the dangerous defects in rotating machinery that lead to destructive and catastrophic scenarios, they occur because of the continuous loads on these rotors, the knowledge of the dynamical behavior of cracked rotor has allowed to recognize the presence of the crack and to stop the rotor in time before catastrophic failures as well as assuring the safety of personnel. Over the past three decades, a large number of research papers on cracked rotor have been published; Comments on cracked rotors can be found in [11-13]. Gasch, R [14] and Edwards, S et al [15] presented excellent reviews in the field of dynamics of cracked rotors and the different procedures to diagnose fracture damages. Davies, W. G. R and Mayes, I. W [16] analyzed the response of a multi-rotor-bearing system containing a transverse crack. Chasalevris, A.C and Papadopoulos, C.A. [17] and Mazanoglu, K et al [18] are studied a multiple cracked shaft where the structure is cracked in at least two positions. The three different crack models, namely, open crack model, breathing crack model, switching crack model are studied in [19-21], these studies show that the breathing crack model is too similar to the reality then the other models. Huang S.C [22] and Sinou, J-J [23] and AL-Shudeifat, M.A et al [24,25] are studied the stability of the cracked rotor using the Floquet theory. The previous studies show that the crack causes a local variation in the stiffness of the cracked rotor's shaft; the main techniques used to formulate this variation are the flexibility matrix method and the time-varying stiffness method. Using the classical version FEM, the flexibility matrix method is the most common technique used to formulate the stiffness matrix of a cracked element of the rotor [26,27]. The time-varying stiffness method is translated by a reduction in the moments of inertia of the cracked element around the axes of rotation, this method has been used in [25,28-29] to study the open crack model and in [23,30-32] to study the breathing crack model.

In our work, we use the hybrid h-p version of the FEM and the time-varying stiffness method to model a rotor with an open transverse crack; this modeling makes it possible to determine the global matrices of the equation of motion. A program was developed in MATLAB to determine the natural and critical frequencies as well as the amplitudes of a cracked rotor. After showing the rapidity of the convergence of the *h-p* version compared to the classical version h of the FEM and the validation of our program results with experimental and theoretical results and other obtained by ANSYS Workbench; a parametric study was provided to show the influence of the depth and the position of the crack on the natural and critical frequencies as well as the amplitudes of a rotor. Finally, a case study of an asymmetric rotor is done to demonstrate that the detection of an open transverse crack in the complex structures of rotors is more difficult compared to simple structures. The remarks and the results of our study can help the maintenance engineers to predict the presence of cracks in rotors and repair them or avoid its failures.

2 EQUATION OF MOTION

In this paper, the Jeffcott rotor model is studied (rigid disk and flexible shaft); the equations of motion are obtained by the application of the Lagrange Eq. (1) on the kinetic and deformation energies of the rotor components (shaft, disk, bearings):

$$\frac{d}{dt}\left(\frac{\partial T}{\partial \dot{q}_i}\right)-\frac{\partial T}{\partial q_i}+\frac{\partial U}{\partial q_i}=F_i \tag{1}$$

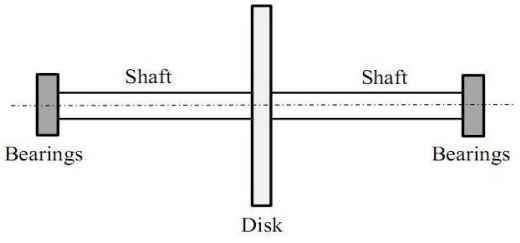

Fig.1
Model of a Jeffcott rotor.

2.1 Kinetic energy of the disk

The expression of the kinetic energy of the disk is given by:

$$T_d = \frac{1}{2} m_d \left(\dot{u}^2 + \dot{w}^2 \right) + \frac{1}{2} I_{dX} \left(\dot{\theta}_X^2 + \dot{\theta}_Z^2 \right) + \frac{1}{2} I_{dY} \left(\Omega^2 + 2\Omega \dot{\theta}_X \theta_Z \right) \tag{2}$$

where

$$I_{dX} = I_{dZ} = \frac{m_d}{12} (3r^2 + 3R^2 + e^2) \tag{3}$$

$$I_{dY} = \frac{m_d}{12} (r^2 + R^2) \tag{4}$$

2.2 Kinetic and deformation energy of the shaft

The expression of the kinetic energy of an element of the shaft with a length L_e is given by:

$$T_a = \frac{1}{2} \rho_a S \int_0^{Le} \left(\dot{u}^2 + \dot{w}^2 \right) dy + \rho_a \frac{I_a}{2} \int_0^{Le} (\dot{\theta}_X^2 + \dot{\theta}_Z^2) dy + \rho_a I_a L_e \Omega^2 + 2\rho_a I_a \Omega \int_0^{Le} \dot{\theta}_X \theta_Z dy \tag{5}$$

The deformation energy of an element of the shaft is calculated by considering the case of an Euler-Bernoulli beam (deformation at the shear force is negligible), this latter is given by:

$$U_a = \frac{E}{2} \int_0^{Le} \left(I_Z \left(\frac{\partial \theta_Z}{\partial y} \right)^2 + I_X \left(\frac{\partial \theta_X}{\partial y} \right)^2 - 2I_{XZ} \frac{\partial \theta_Z}{\partial y} \frac{\partial \theta_X}{\partial y} \right) dy \tag{6}$$

For a healthy element (uncracked element), the moments of inertia of the cross section along the fixed coordinates (*o, X, Z*) are equal to $I_X = I_Z = \pi R^2/4$ and $I_{XZ} = 0$.

In the case of a cracked element; where the cross section is not circular (Fig. 2); the crack causes an asymmetry during the rotation of the rotor (Fig. 2(b)). According to [31], the moments of inertia along the rotating coordinates (*o, x, z*) are given by:

$$\begin{cases} I_x = \dfrac{\pi R^4}{8} + \dfrac{R^4}{4} \left((1-\mu)\left(2\mu^2 - 4\mu + 1\right)\gamma + \sin^{-1}(1-\mu) \right) \\ I_z = \dfrac{\pi R^4}{4} - \dfrac{R^4}{12} \left((1-\mu)\left(2\mu^2 - 4\mu - 3\right)\gamma + 3\sin^{-1}\gamma \right) \\ I_{xz} = 0 \end{cases} \tag{7}$$

where $0 \leq \mu = h/R \leq 1$ is the ratio between the crack depth and the radius of the shaft R (non-dimensional crack depth) and $\gamma = \sqrt{\mu(2-\mu)}$.

According to [33], the moments of inertia along the rotating coordinates with respect to the moments of inertia along the fixed coordinates are:

$$\begin{cases} I_X = I_x \cos^2 \Omega t + I_z \sin^2 \Omega t + 2I_{xz} \cos \Omega t \sin \Omega t \\ I_Z = I_z \cos^2 \Omega t + I_x \sin^2 \Omega t - 2I_{xz} \cos \Omega t \sin \Omega \\ I_{XZ} = (I_z - I_x) \cos \Omega t \sin \Omega t + I_{xz} \left(\cos^2 \Omega t - \sin^2 \Omega t \right) \end{cases} \tag{8}$$

From the Eqs. (6) and (8), we notice that the deformation energy of the cracked element is variable with respect to the element length L_e and also with respect to the time t, therefore, the stiffness of the cracked element depends to the mesh refinement and depends to the time (time-varying stiffness). Consequently, the choice of the number of element of the mesh plays an important role in our study.

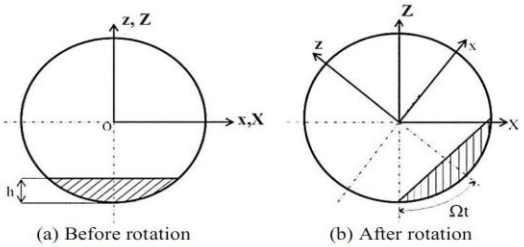

Fig.2
Cross-section of a cracked element.

2.3 Virtual work of the bearings

The components of the generalized forces of the bearings F_u and F_w along the fixed coordinates are given as:

$$\begin{bmatrix} F_u \\ F_w \end{bmatrix} = -\begin{bmatrix} k_{XX} & k_{XZ} \\ k_{ZX} & k_{ZZ} \end{bmatrix}\begin{bmatrix} u \\ w \end{bmatrix} - \begin{bmatrix} c_{XX} & c_{XZ} \\ c_{ZX} & c_{ZZ} \end{bmatrix}\begin{bmatrix} \dot{u} \\ \dot{w} \end{bmatrix} \tag{9}$$

2.4 Unbalance force

The unbalance is characterized by its kinetic energy given by:

$$T_b = m_b d\,\Omega^2 \left(\dot{u}\sin\Omega t - \dot{w}\cos\Omega t \right) \tag{10}$$

where:
m_b: is the mass of the unbalance.
d: is the distance between the position of the unbalance mass and the center.

3 MATRIX FORMULATION BY THE H-P VERSION OF THE FEM

In our finite element modeling by the *h-p* version of the FEM; to develop the elementary matrices of the equation of motion (Appendix), the rotor was discretized into a set of finite elements Euler-Bernoulli beam (Fig. 3), we use the non-dimensional coordinate ξ given by:

$$\xi=(2Y/L_e)-1 \quad , \quad (-1 \le \xi \le 1) \tag{11}$$

The displacements (U, W) and the rotations (θ_X, θ_Z) were replaced by to the vectors of the generalized coordinates and the vectors of the shape functions as:

$$\begin{cases} U = [N_U]\{q_U\} \\ W = [N_W]\{q_W\} \\ \theta_X = [N_{\theta_X}]\{q_{\theta_X}\} \\ \theta_Z = [N_{\theta_Z}]\{q_{\theta_Z}\} \end{cases} \tag{12}$$

where q is the generalized coordinate vector and N is the vector that contains the shape functions and p is the number of degrees of polynomials of an element.

$$\begin{cases} q = \{q_1 q_2 q_3 q_4 \ldots\ldots\ldots\ldots q_p\} \\ N = \{f_1 f_2 f_3 f_4 f_2 \ldots\ldots\ldots\ldots f_p\} \end{cases} \tag{13}$$

The first four functions of the vector N (f_1,f_2,f_3,f_4) are the standard Hermite cubic shape functions of the classical version h which represent the real displacements (U,W) and the rotations (θ_X, θ_Z) of each node of the element [34].

$$\begin{cases} f_1(\xi) = \frac{1}{2} - \frac{3}{4}\xi + \frac{1}{4}\xi^3 \\ f_2(\xi) = \left(\frac{1}{8} - \frac{1}{8}\xi - \frac{1}{8}\xi^2 + \frac{1}{8}\xi^3\right) L_e \\ f_3(\xi) = \frac{1}{2} + \frac{3}{4}\xi - \frac{1}{4}\xi^3 \\ f_4(\xi) = \left(-\frac{1}{8} - \frac{1}{8}\xi + \frac{1}{8}\xi^2 + \frac{1}{8}\xi^3\right) L_e \end{cases} \tag{14}$$

The other components of the vector N where p> 4 are the hierarchical shape functions of the p version of the FEM, these shape functions represent the virtual internal displacement of the element, the functions used in this work are the special Legendre polynomials of Rodrigues [34], which are given by:

$$f_p(\xi) = \sum_{n=0}^{(p-1)/2} \frac{(-1)^n (2p-2n-7)!!}{2^n n!(p-2n-1)!} \xi^{(p-2n-1)} \tag{15}$$

where *p!!=p(p-2)(p-4) .....(2 or 1) , 0!!=(-1)!!=1 and (p-1)/2* designates its own whole part.

After the replacement of the displacements and the rotations by its vector of the shape functions and its generalized coordinates vector in the equation of Lagrange. The size of the elementary matrices of each element is p x p. These matrices are composed of four sub-matrices h, h-p, p-h and p, the assembly of these matrices makes it possible to determine the global matrices of the equation of motion [34]:

$$[M]\ddot{q} + \left([C_p] + \Omega[G]\right)\dot{q} + \left([K_p] + [K]\right)q = F \tag{16}$$

where:

[M] is the global mass matrix which comprises the global mass matrix of the shaft and the disk.

[G] is the global gyroscopic matrix that includes the gyroscopic matrix of the shaft and the disk.

[K] is the global stiffness matrix of the shaft which comprises the stiffness matrix of the cracked element (Appendix) assembled with the matrices of other elements replacing the matrix of the uncracked element by the matrix of cracked element.

$[C_p]$ and $[K_p]$ are the damping and stiffness matrices of the bearings.

q is the vector of generalized coordinates.

F is the vector of unbalance forces,

Ω is the rotation speed in *rd/s*.

The forward and backward natural and critical speeds are obtained from the eigen solution of the matrix S given as:

$$S(\Omega) = \begin{bmatrix} 0 & I \\ -[M]^{-1}\left([K] + [K_p]\right) & -[M]^{-1}\left(\Omega[G] + [C_p]\right) \end{bmatrix} \tag{17}$$

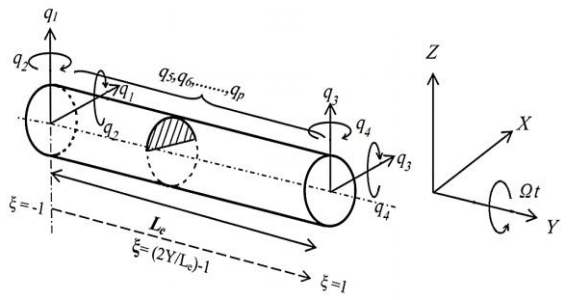

Fig.3
Beam element with circular section.

4 VALIDATION

The rotor studied in our work is the one studied by AL-Shudeifat, M.A [25] (Figs. 4,5), the physical parameters of this rotor are given in Table 1:

Table 1
Physical parameters of the rotor studied.

Young's Module (E)	2.1e11 N/m^2
Length of the shaft (L)	0.724 m
Radius of the shaft (R)	7.95e-3 m
Density of the shaft (ρ_a)	7800 kg/m^3 (Steel)
Number of disks	2
Position of the disk 1	0.124 m (from the left bearings)
Position of the disk 2	0.6 m (from the left bearings)
Inner radius of the disks (R)	7.95e-3 m
External radius of the disks (r)	76.2e-3 m
Thickness of the disks (e)	11.72e-3 m
Density of the disk (ρ_d)	2700 kg/m^3(Aluminum)
Stiffness of bearings (k_{xx},k_{zz})	7e7 N/m
Damping of bearings (c_{xx},c_{zz})	5e2 Ns/m
Mass unbalance (m_b)	10^{-6} $kg.m$
Mass unbalance angle (ψ)	$\pi/2$ rd

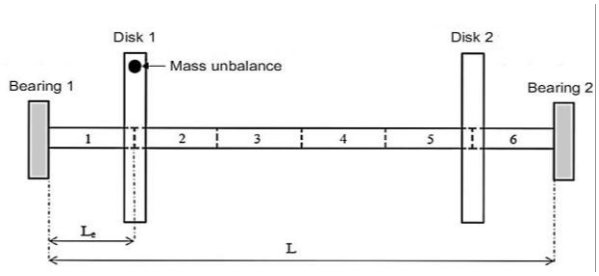

Fig.4
Finite element model of the rotor studied.

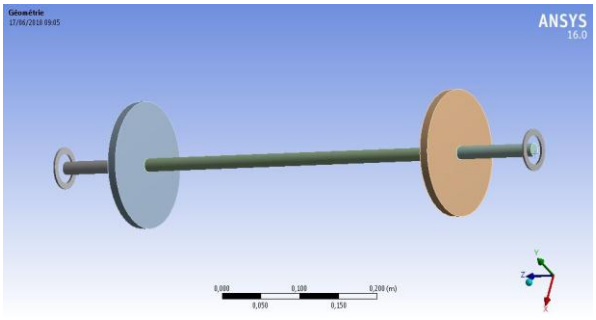

Fig.5
The studied rotor model in ANSYS Worbench.

4.1 Convergence study

The convergence study is done to show the rapidity of the convergence of the *h-p* version compared to the classical version *h*. This study is done in the stationary state of the rotor (Ω=0). The characteristics of the rotor model studied are given in Table 1.

4.1.1 Convergence of the h version of the FEM

The convergence of the classical version *h* of the FEM is obtained by increasing the number of elements (refinement of mesh). The convergence of the first three modes is represented in Table 2., and the results of this table are illustrated in the Figs. 6, 7, 8.

Table 2
Convergence of the first three modes according to the number of elements - *h* version -.

Mode	Number of elements (*n*)					
	n=6	*n*=12	*n*=18	*n*=24	*n*=36	*n*=48
1	49.0161	49.0152	49.0151	49.0151	49.0151	49.0151
2	150.1712	150.1556	150.1548	150.1546	150.1546	150.1545
3	353.4762	353.1575	353.1397	353.1366	353.1355	353.1353

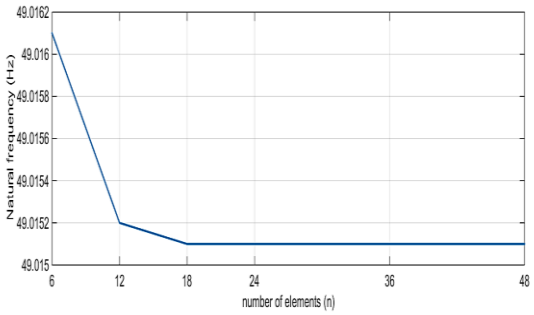

Fig.6
Convergence curve of the first mode - *h* version -.

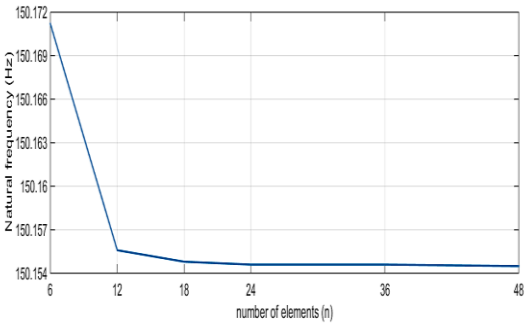

Fig.7
Convergence curve of the second mode - *h* version -.

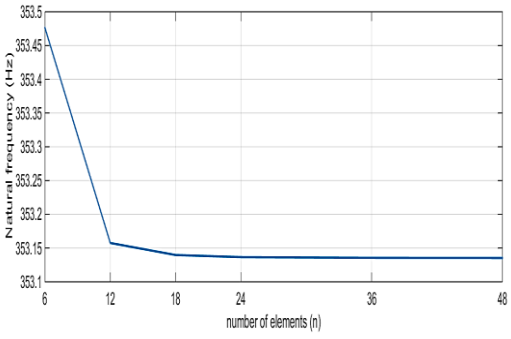

Fig.8
Convergence curve of the third mode - *h* version -.

4.1.2 Convergence of the h-p version of the FEM

Table 3., shows the convergence of the *h-p* version of the three first modes, the convergence is obtained by fixing the number of elements to 6 (Fig. 4) and by varying the number of degree of polynomials, the results of this table are illustrated in the Figs. 9, 10, 11.

Table 2., and Figs. 6, 7, 8 show that, in the case of the classical version *h* of the FEM, the natural frequencies converge from 18 elements for the first mode and 24 elements for the second and third modes.

In the case of the *h-p* version of the FEM, Table 3., and Figs. 9, 10, 11 show that for a rotor discretized into 6 elements, the natural frequencies of the first three modes converge from 6 degrees of polynomials μ.

The convergence study represents the rapidity of the convergence of the *h-p* version compared to the *h* version of FEM. The studied rotor will be discretized into 6 elements by taking a degree of polynomial $p = 6$ (Fig. 4).

Table 3
Convergence of the first three modes according to the number of degrees of polynomials - *h-p* version -.

Mode	Degree of polynomials (p)					
	p=5	p=6	p=7	p=8	p=9	p=10
1	49.0152	49.0151	49.0151	49.0151	49.0151	49.0151
2	150.1547	150.1545	150.1545	150.1545	150.1545	150.1545
3	353.1396	353.1353	353.1352	353.1352	353.1352	353.1352

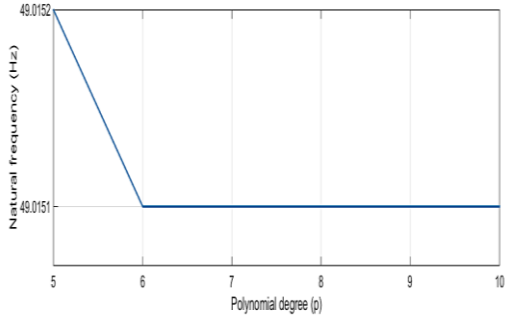

Fig.9
Convergence curve of the first mode - *h-p* version -.

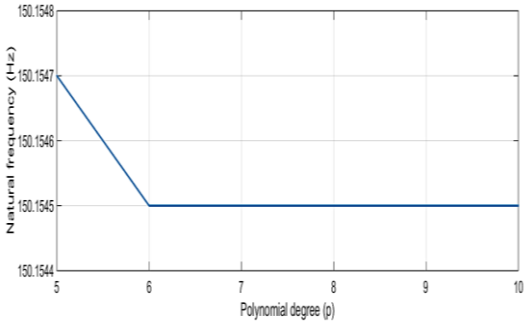

Fig.10
Convergence curve of the second mode - *h-p* version -.

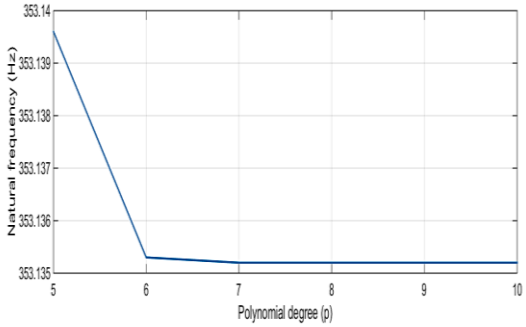

Fig.11
Convergence curve of the third mode - *h-p* version -.

4.2 Validation of results

Table 4., represents the comparison between the first backward and forward critical speed determined by the *h-p* version of the FEM and the values of the critical speeds determined experimentally by AL-Shudeifat M.A [25] and by the classical version of the FEM and also with a results generated by the simulator ANSYS Workbench (Fig. 5), to approximate to the experimental, we decrease the influence of the stiffness of the cracked element by the increase of the number of element (n=12),

The error percentage between the results obtained by the *h-p* version of the FEM and the other results do not exceed 3%, that prove the efficiency of the *h-p* version of the FEM and the time-varying stiffness method in the study of the cracked rotors, and also the reliability of our MATLAB program, with this program we can perform simulations for variable values of depths and positions of the crack.

Table 4
Comparison between the results of the *h-p* version of the FEM and other theoretical, numerical and experimental results.

Mode	Backward	Forward					
Non-dimensional crack depth (μ)	0	0.15	0.3	0.45	0.6	0.75	1
h-p version of FEM	2863.8	3029.3	3012	2990.8	2967	2940.7	2888.9
Experimental	2870	3062	3050	3037	3015	2995	2970
h version of FEM	2863.5	3013.7	2996.5	2975.5	2951.8	2925.6	2874
ANSYS Workbench	2870.5	3018.7	3016.6	2992.5	2988.3	2989.2	2980.8
$\varepsilon_{h\text{-}p/Exp}$ (%)	0.21	1.06	1.24	1.52	1.59	1.81	2.73
$\varepsilon_{h\text{-}p/h}$ (%)	0.01	0.5	0.5	0.51	0.51	0.52	0.52
$\varepsilon_{h\text{-}p/\text{ANSYS Workbench}}$ (%)	0.23	0.35	0.15	0.05	0.71	1.62	3

5 FREQUENCY ANALYSIS

5.1 Study in the stationary state ($\Omega = 0$*)*

In this part, we study the influence of the depth and the position of the crack on the natural frequencies of the rotor; with varying the depth, as well as the position of the crack (Fig. 4).

Tables 5, 6, 7 represent the variation of the natural frequencies of the first three modes with respect to the depth of the crack in the case where the crack is located in the first, second or third element, and the results of these tables are illustrated in Figs. 12 to 20.

Tables 5, 6, 7 and Figs. 12-20 show that the natural frequencies of the backward and forward modes of a cracked rotor decrease with respect to that of an uncracked rotor, this decrease is slight in forward modes by that in backward modes, the diverge between the frequencies of the forward and backward modes is because of the asymmetry in the geometry of rotor caused by the crack.

The natural frequencies decrease more the crack depth propagates, and in any crack position the natural frequencies decrease rapidly from the depth (μ = 0.4); this because of the decrease of the stiffness of the cracked element.

For the frequencies of the first mode, more the crack approach to the middle of the shaft the frequencies decrease and the degree of severity of the crack become very important. In the case of the second mode, the natural frequencies take its minimum value when the crack located in the second element; consequently, the variation curve of the natural frequencies with respect to the position of the crack is similar to the mode of deformation of the rotor.

Table 5
Variation of the natural frequencies of first three modes with respect to the crack depth in the case where the crack is located in the first element.

Mode		Non-dimensional crack depth (μ)										
		0	0.1	0.2	0.3	0.4	0.5	0.6	0.7	0.8	0.9	1
1	backward	49.02	48.97	48.87	48.74	48.55	48.3	47.98	47.56	47.04	46.4	45.65
	forward	49.02	48.99	48.96	48.94	48.92	48.9	48.88	48.86	48.84	48.8	48.74
2	backward	150.2	149.7	148.8	147.4	145.6	143.3	140.5	137.1	133.1	128.6	124.1
	forward	150.2	149.9	149.6	149.4	149.2	149	148.9	148.7	148.4	148	147.5
3	backward	353.1	351.5	348.1	343.4	337.5	330.3	322.1	312.2	304	295.1	287.3
	forward	353.1	352.3	351.2	350.3	349.6	349	348.4	347.8	346.9	345.5	343.6

Table 6
Variation of the natural frequencies of first three modes with respect to the crack depth in the case where the crack is located in the second element.

	Mode	Non-dimensional crack depth (μ)										
		0	0.1	0.2	0.3	0.4	0.5	0.6	0.7	0.8	0.9	1
1	backward	49.02	48.8	48.37	47.75	46.94	45.91	44.64	43.11	41.35	39.41	37.39
	forward	49.02	48.9	48.77	48.65	48.56	48.49	48.41	48.32	48.2	48.03	47.78
2	backward	150.2	149.1	147	144.3	140.9	137.1	133	128.7	124.4	120.3	116.7
	forward	150.2	149.6	148.9	148.4	147.9	147.6	147.2	146.8	146.3	145.5	144.4
3	backward	353.1	352.1	350	347.3	343.9	339.9	335.3	330.2	324.5	318.3	311.6
	forward	353.1	352.6	351.9	351.4	350.9	350.6	350.2	349.8	349.3	348.5	347.4

Table 7
Variation of the natural frequencies of first three modes with respect to the crack depth in the case where the crack is located in the third element.

	Mode	Non-dimensional crack depth (μ)										
		0	0.1	0.2	0.3	0.4	0.5	0.6	0.7	0.8	0.9	1
1	backward	49.02	48.7	48.08	47.2	46.08	44.7	43.07	41.19	39.11	36.91	34.71
	forward	49.02	48.85	48.65	48.49	48.35	48.24	48.14	48.01	47.84	47.59	47.24
2	backward	150.2	149.9	149.5	148.9	148.2	147.3	146.2	145	143.7	142.3	140.8
	forward	150.2	150	149.9	149.8	149.7	149.6	149.6	149.5	149.4	149.2	149
3	backward	353.1	351.8	349.2	345.7	341.3	336.4	330.8	324.9	318.8	312.7	307
	forward	353.1	352.4	351.6	350.9	350.3	349.9	349.4	348.9	348.2	347.2	345.8

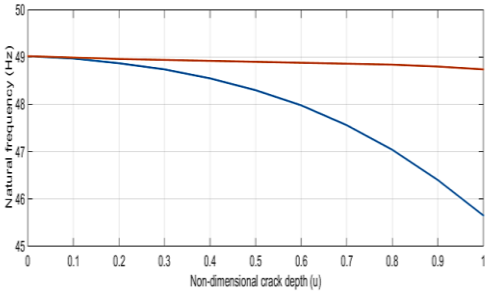

Fig.12
Variation curve of the natural frequencies of the first mode (backward –Blue- and forward –Red-) with respect to the non-dimensional crack depth in the case where the crack is located in the first element.

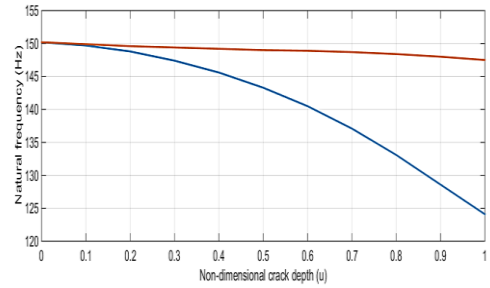

Fig.13
Variation curve of the natural frequencies of the second mode (backward –Blue- and forward –Red-) with respect to the non-dimensional crack depth in the case where the crack is located in the first element.

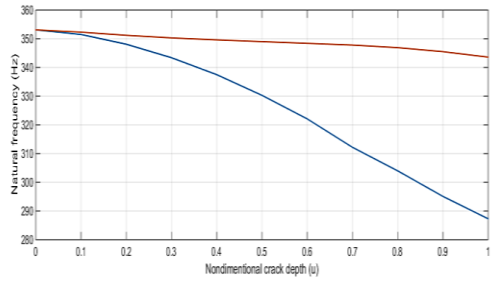

Fig.14
Variation curve of the natural frequencies of the third mode (backward –Blue- and forward –Red-) with respect to the non-dimensional crack depth in the case where the crack is located in the first element.

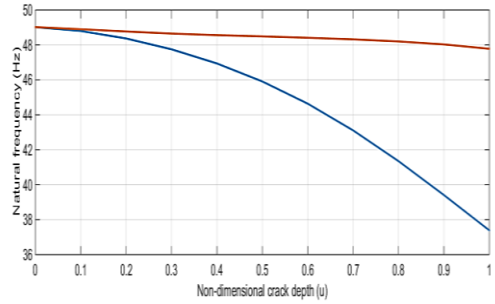

Fig.15
Variation curve of the natural frequencies of the first mode (backward –Blue- and forward –Red-) with respect to the non-dimensional crack depth in the case where the crack is located in the second element.

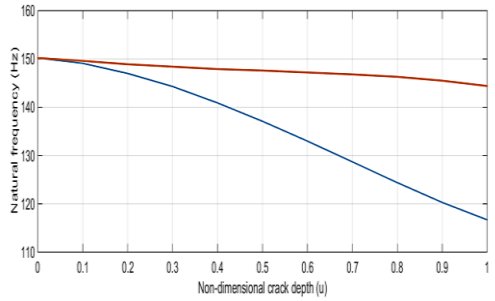

Fig.16
Variation curve of the natural frequencies of the second mode(backward –Blue- and forward –Red-) with respect to the non-dimensional crack depth in the case where the crack is located in the second element.

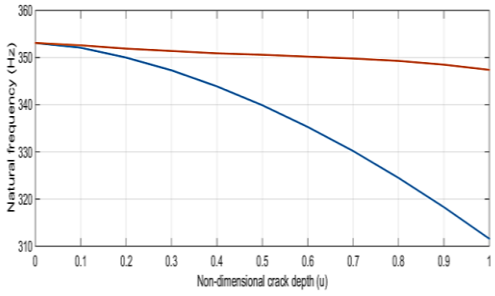

Fig.17
Variation curve of the natural frequencies of the third mode (backward –Blue- and forward –Red-) with respect to the non-dimensional crack depth in the case where the crack is located in the second element.

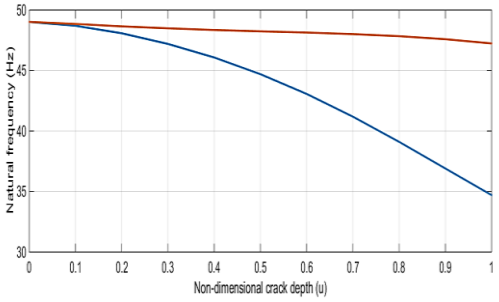

Fig.18
Variation curve of the natural frequencies of the first mode (backward –Blue- and forward –Red-) with respect to the non-dimensional crack depth in the case where the crack is located in the third element.

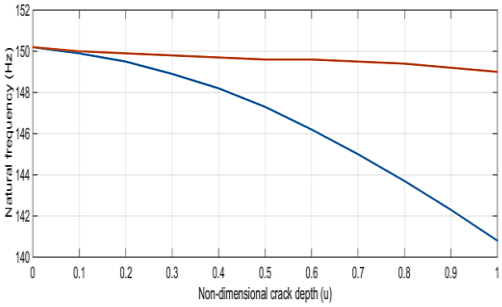

Fig.19
Variation curve of the natural frequencies of the second mode (backward –Blue- and forward –Red-) with respect to the non-dimensional crack depth in the case where the crack is located in the third element.

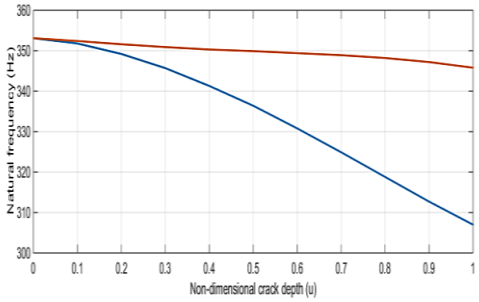

Fig.20
Variation curve of the natural frequencies of the third mode (backward –Blue- and forward –Red-) with respect to the non-dimensional crack depth in the case where the crack is located in the third element.

5.2 Study in the rotational state ($\Omega \neq 0$)

In the rotational state, we study the effect of the depth and the position of the crack on the critical frequencies of the rotor.

In Tables 8, 9, 10, we represent the values of the critical frequencies of the first three modes according to the non-dimensional crack depth in the case where the crack is located in the first, second or third element, and the results of these tables are illustrated in Figs. 21 to 29.

The comments on the variation of the critical frequencies with respect to the depth and the position of the crack are the same comments of the variation of the natural frequencies in the stationary state.

Table 8
Variation of the critical frequencies of first three modes with respect to the crack depth in the case where the crack is located in the first element.

	Mode	Non-dimensional crack depth (μ)										
		0	0.1	0.2	0.3	0.4	0.5	0.6	0.7	0.8	0.9	1
1	backward	47.73	47.7	47.65	47.57	47.47	47.32	47.13	46.87	46.48	45.98	45.33
	forward	50.4	50.37	50.3	50.2	50.08	49.95	49.82	49.65	49.47	49.28	49.12
2	backward	147.2	146.9	146.4	145.6	144.3	142.5	140	136.8	132.9	128.6	124.1
	forward	152.9	152.5	151.8	151	150.3	149.7	149.2	148.8	148.3	147.9	147.3
3	backward	345.3	343.6	340.5	336.1	330.3	322.9	314.4	304.9	295.3	286.1	277.6
	forward	358.4	357.4	355.8	354.1	352.8	351.6	350.6	349.8	348.8	347.2	345.8

Table 9
Variation of the critical frequencies of the first mode with respect to the crack depth in the case where the crack is located in the second element.

	Mode	Non-dimensional crack depth (μ)										
		0	0.1	0.2	0.3	0.4	0.5	0.6	0.7	0.8	0.9	1
1	backward	47.73	47.55	47.27	46.83	46.25	45.4	44.27	42.85	41.17	39.25	37.32
	forward	50.4	50.25	49.97	49.67	49.37	49.1	48.9	48.7	48.48	48.3	48.02
2	backward	147.2	146.3	144.8	142.6	139.7	136.1	132.2	128.1	123.8	119.8	116.3
	forward	152.9	152.2	151	149.9	149	148.4	147.9	147.3	146.8	146	144.8
3	backward	345.3	344.7	343.7	342.3	340.2	337.4	333.7	329.2	323.8	317.8	311.3
	forward	358.4	357.4	355.8	354	352.3	350.9	349.8	348.9	348	347.1	345.9

Table 10
Variation of the critical frequencies of first three modes with respect to the crack depth in the case where the crack is located in the third element.

	Mode	Non-dimensional crack depth (μ)										
		0	0.1	0.2	0.3	0.4	0.5	0.6	0.7	0.8	0.9	1
1	backward	47.73	47.48	47.05	46.45	45.53	44.33	42.83	41.02	38.98	36.78	34.68
	forward	50.4	50.15	49.77	49.37	48.98	48.72	48.5	48.28	48.05	47.8	47.42
2	backward	147.2	147	146.8	146.4	145.9	145.3	144.5	143.5	142.3	141.1	139.8
	forward	152.9	152.8	152.5	152.2	151.8	151.5	151.2	150.9	150.6	150.3	149.9
3	backward	345.3	344.4	342.8	340.6	337.6	333.7	328.9	323.5	317.8	311.9	306.4
	forward	358.4	357.3	355.5	353.6	351.9	350.5	349.5	348.5	347.4	346.2	344.9

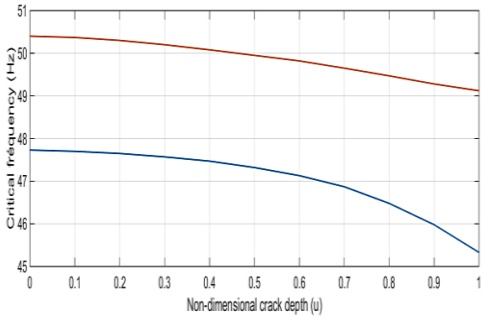

Fig.21
Variation curve of the critical frequencies of the first mode (backward –Blue- and forward –Red-) with respect to the non-dimensional crack depth in the case where the crack is located in the first element.

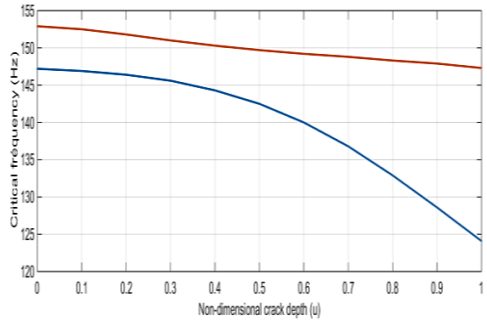

Fig.22
Variation curve of the critical frequencies of the second mode (backward –Blue- and forward –Red-) with respect to the crack non-dimensional depth in the case where the crack is located in the first element.

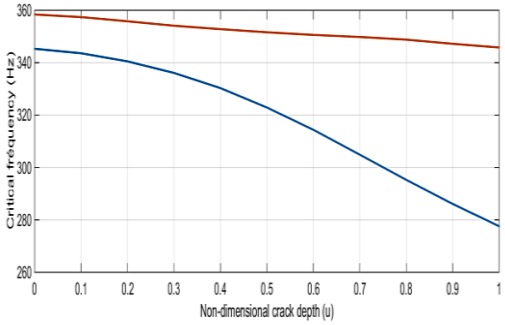

Fig.23
Variation curve of the critical frequencies of the third mode (backward –Blue- and forward –Red-) with respect to the non-dimensional crack depth in the case where the crack is located in the first element.

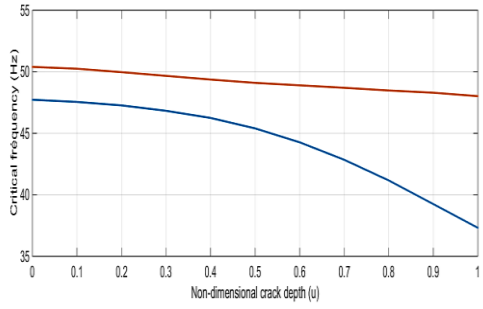

Fig.24
Variation curve of the critical frequencies of the first mode (backward –Blue- and forward –Red-) with respect to the crack non-dimensional depth in the case where the crack is located the second element.

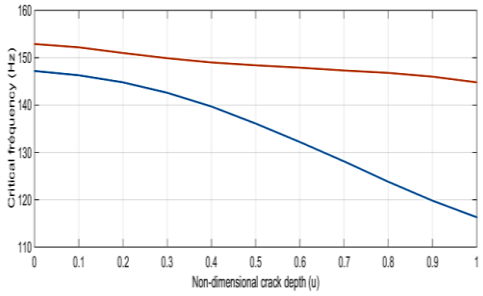

Fig.25
Variation curve of the critical frequencies of the second mode (backward –Blue- and forward –Red-) with respect to the non-dimensional crack depth in the case where the crack is located in the second element.

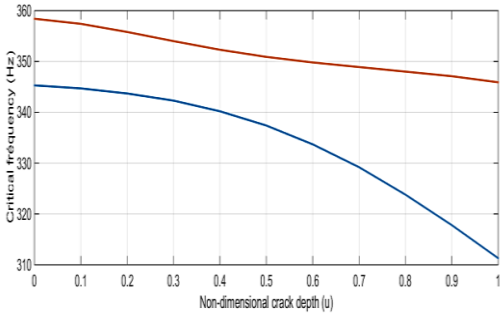

Fig.26
Variation curve of the critical frequencies of the third mode (backward –Blue- and forward –Red-) with respect to the non-dimensional crack depth in the case where the crack is located in the second element.

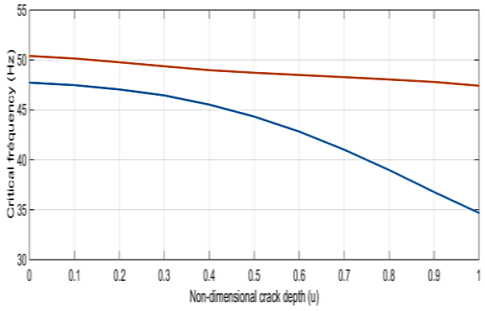

Fig.27
Variation curve of the critical frequencies of the first mode (backward –Blue- and forward –Red-)with respect to the non-dimensional crack depth in the case where the crack is located in the third element.

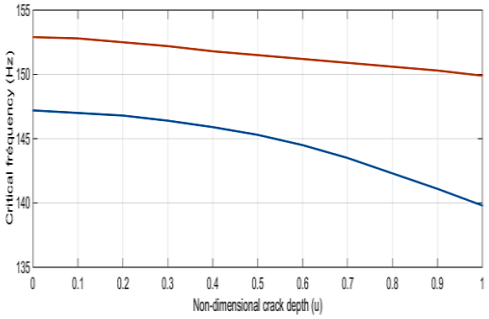

Fig.28
Variation curve of the critical frequencies of the second mode (backward –Blue- and forward –Red-) with respect to the non-dimensional crack depth in the case where the crack is located in the third element.

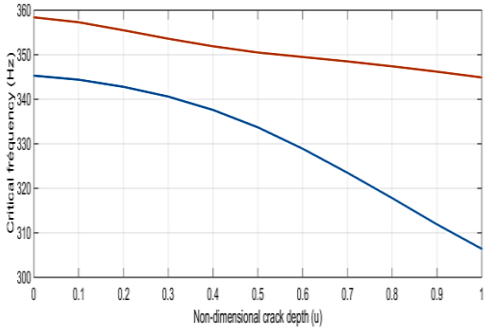

Fig.29
Variation curve of the critical frequencies of the third mode (backward –Blue- and forward –Red-) with respect to the non-dimensional crack depth in the case where the crack is located in the third element.

6 SPECTRAL ANALYSIS

In this analysis, we study the influence of the depth and position of the crack on the vertical displacement (along the Z axis) of the rotor in a given node.

Fig. 30 shows the difference between the vertical amplitude at the third node from the left bearing of a healthy rotor (blue curve) and a cracked rotor (red curve) where the ratio of crack depth $\mu = 0.3$ and the crack is located in the second element.

Figs. 31, 32, 33 represent the waterfall of variation of the vertical amplitudes at the fourth node with respect to the crack depth and the rotational speed in the case where the crack is located in the first, second and third element. The offset of the amplitudes of the cracked rotor relative to the healthy rotor involves a decrease in critical speeds which is caused by a decrease in the stiffness of the rotor.

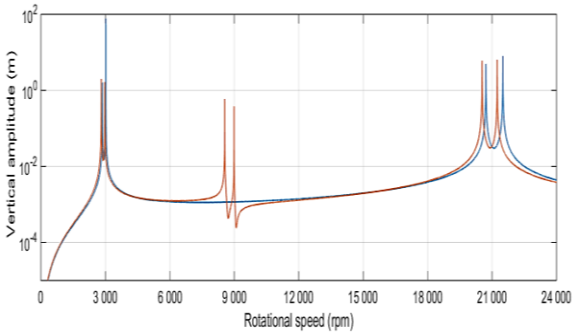

Fig.30
Vertical amplitude of an uncracked rotor (blue) with cracked rotor (red) in the case where the crack is located in the second element and $\mu = 0.3$.

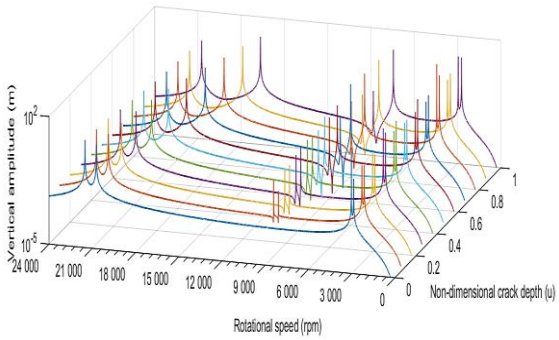

Fig.31
Waterfall of the vertical amplitudes where the crack is located in the first element.

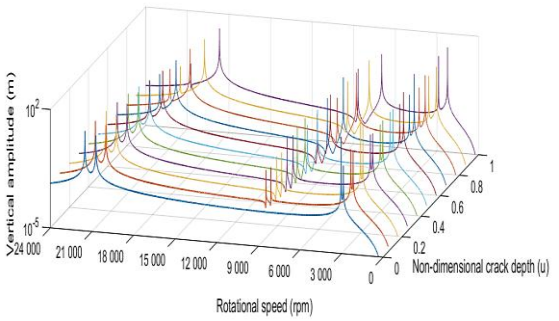

Fig.32
Waterfall of the vertical amplitudes where the crack is located in the second element.

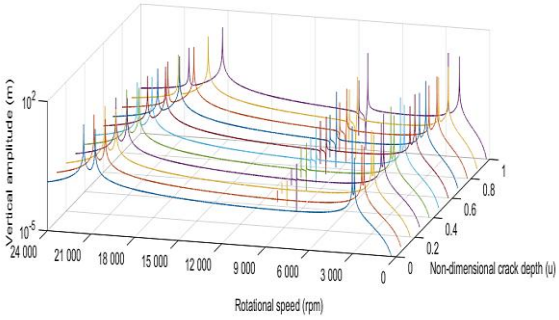

Fig.33
Waterfall of the vertical amplitudes where the crack is located in the third element.

7 CASE STUDY OF AN ASYMMETRIC ROTOR

In this part, we study an asymmetrical rotor where the crack detection is more difficult compared to symmetrical rotor. Because in the case of the symmetric, we can do the diagnosis on the half of the rotor and the results founded are identical for the two sides.

The characteristics of the rotor studied in this case are the same as those of the rotor studied previously (Table 1); the difference is in the number, the radius and the positions of the disks. The first disc is located in the right of the first element and its outer radius is 1/3 of the outer radius of the third disk. The second disk is located in the middle of the shaft and its outer radius is 1/2 of outer radius of the third disk. The last disk is located in the left of the sixth element and its outer radius is 76.2e-3 *m*, the three disks are in aluminum, (Fig. 34).

In Table 11., and Fig. 35, we respectively represent the variations of the critical frequencies of the first three modes and the vertical amplitudes with respect to the position of the crack. We notice a clear difference between the right side and the left side of the rotor; consequently, the detection of the crack in the case of asymmetric geometry of rotor is difficult more than the symmetric rotor.

Table 11
Variation of the critical frequencies modes with respect to the position of the crack in the case where μ=0.5.

Mode		Cracked element					
		1	2	3	4	5	6
1	backward	47.88	45.5	44.18	44.55	46.53	48.12
	forward	49.37	48.7	48.33	48.42	48.88	49.57
2	backward	168.8	162.1	176.3	172.2	166.4	174.5
	forward	177.9	176.6	180.6	179.1	177.7	179.8
3	backward	355.8	376.4	362.4	373.5	363	365.8
	forward	389.5	388.4	384.9	388	384.3	385.6

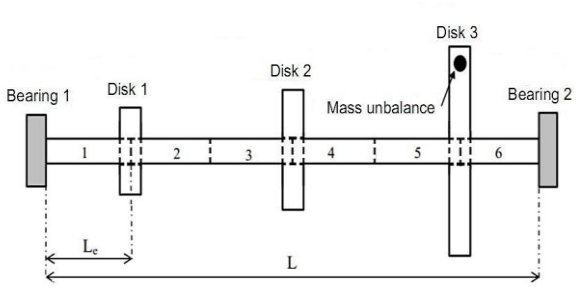

Fig.34
Finite element model of an asymmetrical rotor.

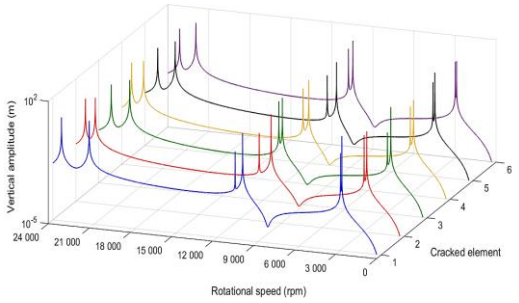

Fig.35
Waterfall of vertical amplitudes at the third node from the left where μ =0.5.

8 CONCLUSIONS

In this work, we studied the effect of an open transverse crack on the vibratory behavior of a rotor, using the *h-p* version of the FEM; we used the time-varying stiffness method to determine the stiffness of the cracked element. A

program was developed in MATLAB to identify the natural and critical frequencies as well as the amplitudes of a cracked and uncracked rotor. After showing the rapidity of convergence of the *h-p* version compared to the classical version h of the FEM and the validation of our program results with numerical and experimental results, we are studied the effect of the position and the depth of the crack on the natural and critical frequencies and on the amplitudes of a symmetrical and asymmetrical rotor; we noticed that:

- The *h-p* version of the FEM and the time-varying stiffness method are appropriate for the study of the cracked rotors especially in the case of continuous geometries.
- The crack causes a decrease in stiffness of the cracked element of the shaft.
- The stiffness of the cracked element depends to the length of the cracked rotor and depends to the mesh refinement.
- The stiffness of the cracked element depends to the crack depth.
- The natural and critical frequencies of a cracked and uncracked rotor have a gap that can be used to identify the presence and depth and position of the crack.
- The natural and critical frequencies of the backward and forward modes of the cracked rotor decrease with respect to that of the uncracked rotor.
- The crack causes an asymmetry in the geometry of the rotor.
- The natural and critical frequencies decrease with the increase of the crack depth, this decrease becomes very rapid from the depth μ=0.4, this because of the decrease of the stiffness of the cracked element.
- The variation curve of natural and critical frequencies with respect to the position of the crack is similar to the shape of deformation mode.
- The results found show that the detection of the crack is difficult because we can find many theoretical results which have the same values, this because of the refinement of mesh. The *h-p* version makes it possible to reduce the number of mesh elements, which leads to the limitation of the possibilities of finding identical values for different positions and depths.
- Spectral analysis is a complement to the frequency analysis; it can help to find the difference between several cases found by the frequency analysis.
- The detection of the cracks in the case of symmetric rotors is easy then complex rotors.

The previous remarks can help the maintenance engineers to predict the presence of cracks in rotors and repair them or avoid its failures

APPENDIX

The elementary matrices of the rotor components (shaft-disk-bearing) are given as:

1 SHAFT

1.1 Mass matrix

$$\left[M_e^{shaft}\right]=\begin{bmatrix} M_U^{shaft} & 0 \\ 0 & M_W^{shaft} \end{bmatrix}$$

where

$$\left[M_W^{shaft}\right]=\rho_a S\int_0^{Le}\left[N_W\right]^2 dy+\rho_a I_a\int_0^{Le}\left[\frac{d\left[N_W\right]}{dy}\right]^2 dy$$

$$\left[M_U^{shaft}\right]=\rho_a S\int_0^{Le}\left[N_U\right]^2 dy+\rho_a I_a\int_0^{Le}\left[\frac{d\left[N_U\right]}{dy}\right]^2 dy$$

$$\theta_X=\frac{\partial W}{\partial y}\quad,\quad \theta_Z=\frac{\partial U}{\partial y}$$

1.2 Gyroscopic matrix

$$\left[G_e^{shaft}\right]=\begin{bmatrix} 0 & G^{shaft} \\ -G^{shaft} & 0 \end{bmatrix}$$

where

$$\left[G^{shaft}\right]=2\rho_a I_a \int_0^{Le}\left[\left[\frac{d\left[N_U\right]}{dy}\right]\left[\frac{d\left[N_W\right]}{dy}\right]\right]dy$$

1.3 Stiffness matrix
1.1.3 The stiffness matrix of the uncracked element

$$\left[K_e^{shaft}\right]=\begin{bmatrix} K_U^{shaft} & 0 \\ 0 & K_W^{shaft} \end{bmatrix}$$

where

$$\left[K_U^{shaft}\right]=EI_a \int_0^{Le}\left[\frac{d^2\left[N_U\right]}{dy^2}\right]^2 dy$$

$$\left[K_W^{shaft}\right]=EI_a \int_0^{Le}\left[\frac{d^2\left[N_W\right]}{dy^2}\right]^2 dy$$

1.2.3 The stiffness matrix of the cracked element

$$\left[K^{crack}\right]=\begin{bmatrix} K_U^{crack} & K_{UW}^{crack} \\ K_{WU}^{crack} & K_W^{crack} \end{bmatrix}$$

where

$$\left[K_U^{crack}\right]=EI_X \int_0^{Le}\left[\frac{d^2\left[N_U\right]}{dy^2}\right]^2 dy$$

$$\left[K_W^{crack}\right]=EI_Z \int_0^{Le}\left[\frac{d^2\left[N_U\right]}{dy^2}\right]^2 dy$$

$$\left[K_{UW}^{crack}\right]=\left[K_{WU}^{crack}\right]=-2EI_{XZ} \int_0^{Le}\left[\left[\frac{d^2\left[N_U\right]}{dy^2}\right]\left[\frac{d^2\left[N_W\right]}{dy^2}\right]\right]dy$$

2 DISK

The disks are fixed between two element of the shaft where ξ=1 or ξ=-1.

2.1 Mass matrix

$$\left[M_e^{disk}\right]=\begin{bmatrix} M_U^{disk} & 0 \\ 0 & M_W^{disk} \end{bmatrix}$$

where

$$\left[M_U^{disk}\right]=m_d\left[N_U\right]^2+I_{dX}\left[\frac{d\left[N_U\right]}{dy}\right]^2$$

$$\left[M_W^{disk}\right]=m_d\left[N_W\right]^2+I_{dZ}\left[\frac{d\left[N_W\right]}{dy}\right]^2$$

$$I_{dX}=I_{dZ}=\frac{m_d}{12}(3R^2+3r^2+e^2)$$

2.2 Gyroscopic matrix

$$\left[G_e^{disk}\right]=\begin{bmatrix} 0 & G^{disk} \\ -G^{disk} & 0 \end{bmatrix}$$

where

$$\left[G^{disk}\right]=I_{dY}\left[\frac{d\left[N_U\right]}{dy}\right]\left[\frac{d\left[N_W\right]}{dy}\right]$$

$$I_{dY}=\frac{m_d}{12}(r^2+R^2)$$

3 BEARING

$$\left[K_p\right]=\begin{bmatrix} k_{XX} & k_{XZ} \\ k_{ZX} & k_{ZZ} \end{bmatrix}\quad,\quad \left[C_p\right]=\begin{bmatrix} c_{XX} & c_{XZ} \\ c_{ZX} & c_{ZZ} \end{bmatrix}$$

REFERENCES

[1] Gallagher R.H., 1975, *Finite Element Analysis: Fundamentals*, Prentice Hall Civil Engineering and Engineering Mechanics, Pearson College Div.

[2] Zienkiewicz C., 1977, *The Finite Element Method*, McGraw-Hill.

[3] Szabo B.A., 1979, Some recent developments in the finite element analysis, *Computers & Mathematics Applications*, **5**(2): 99-115.

[4] Babuška I., Szabo B.A., Katz I.N., 1981, The *p*-version of the finite element method, *SIAM Journal on Numerical Analysis* **18**(3): 515-545.

[5] Meirovitch L., Bahuh H., 1983, On the inclusion principle for the hierarchical finite element method, *International Journal for Numerical Methods in Engineering* **19**: 281-291.

[6] Gui W., Babuška I., 1986, The *h, p* and *h-p* versions of the finite element method in 1 dimension, part I, The error analysis of the *p*-version, *Numerische Mathematik* **49**(6): 577-612.

[7] Babuška I., Suri M., 1987, The *h-p* version of the finite element method with quasi uniform meshes, *Mathematical Modeling and Numerical Analysis* **21**(2): 199-238.

[8] Babuška I., Guo B.Q., 1992, The *h, p* and *h-p* version of the finite element method: Basis theory and applications, *Advances in Engineering Software* **15** (3-5): 159-174.

[9] Boukhalfa A., Hadjoui A., 2010, Free vibration analysis of an embarked rotating composite shaft using the *h-p* version of the FEM, *Latin American Journal of Solids and Structures* **7**(2): 105-141.
[10] Saimi A., Hadjoui A., 2016, An engineering application of the h-p version of the finite elements method to the dynamics analysis of a symmetrical on-board rotor, *European Journal of Computational Mechanics* **25**(5): 1779-7179.
[11] Wauer J., 1990, Dynamics of cracked rotors: literature survey, *Applied Mechanics Reviews* **43**(1): 13-17.
[12] Dimarogonas A.D., 1996, Vibration of cracked structures: a state of the art review, *Engineering Fracture Mechanics* **55**(5): 831-857.
[13] Sabnavis G., Kirk R.G., Kasarda M., Quinn D.D., 2004, Cracked shaft detection and diagnostics: a literature review, *The Shock and Vibration Digest* **36**(4): 287-296.
[14] Gasch R., 1993, A survey of the dynamic behavior of a simple rotating shaft with a transverse crack, *Journal of Sound and Vibration* **160**: 313-332.
[15] Edwards S., Lees A. W., Friswell M. I., 1998, Fault diagnosis of rotating machinery, *The Shock and Vibration Digest* **30**: 4-13.
[16] Davies W. G. R., Mayes I. W., 1984, The vibration behavior of a multi-shaft, multi-bearing system in the presence of a propagating transverse crack, *Journal of Vibration, Acoustics, Stress, and Reliability in Design* **106**: 146-153.
[17] Chasalevris A.C., Papadopoulos C.A., 2008, Coupled horizontal and vertical vibrations of a stationary shaft with two cracks, *Journal of Sound and Vibration* **309**: 507-528.
[18] Mazanoglu K., Yesilyurt I., Sabuncu M., 2009, Vibration analysis of multiple-cracked non-uniform beams, *Journal of Sound and Vibration* **320**(4–5): 977-989.
[19] Darpe A.K., Gupta K., Chawla A., 2004, Transient response and breathing behaviour of a cracked Jeffcott rotor, *Journal of Sound and Vibration* **272**: 207-243.
[20] Petal T.H., Darpe A.K., 2008, Influence of crack breathing model on nonlinear dynamics of a cracked rotor, *Journal of Sound and Vibration* **311**: 953-972.
[21] AL-Shudeifat M.A., Eric A., Butcher Carl R.S., 2010, General harmonic balance solution of a cracked rotor-bearing-disk system for harmonic and sub-harmonic analysis: Analytical and experimental approach, *International Journal of Engineering Science* **48**: 921-935.
[22] Huang S.C., Huang Y.M., Shiah S.M., 1993, Vibration and stability of a rotating shaft containing a transverse crack, *Journal of Sound Vibration* **162**: 387-401.
[23] Sinou J-J., 2007, Effects of a crack on the stability of a non-linear rotor system, *International Journal of Non-Linear Mechanics* **42**(7): 959-972.
[24] Guo C., AL-Shudeifat M.A., Yan J., Bergman L.A., McFarland D.M., Butcher E.A., 2013, Stability analysis for transverse breathing cracks in rotor systems, *European Journal of Mechanics and Solids* **42**: 27-34.
[25] AL-Shudeifat M.A., 2015, Stability analysis and backward whirl investigation of cracked rotors with time-varying stiffness, *Journal of Sound and Vibration* **348**: 365-380.
[26] Dimarogonas A.D., Papadopoulos C.A., 1983, Vibration of cracked shafts in bending, *Journal of Sound and Vibration* **91**(4): 583-593.
[27] Silani M., Ziaei-Rad S., Talebi H., 2013, Vibration analysis of rotating systems with open and breathing cracks, *Applied Mathematical Modeling* **37**(24): 9907-9921.
[28] AL-Shudeifat M.A., 2013, On the finite element modeling of an asymmetric cracked rotor, *Journal of Sound and Vibration* **332**(11): 2795-2807.
[29] Qinkai H., Fulei C., 2013, Dynamic response of cracked rotor-bearing system under time-dependent base movements, *Journal of Sound and Vibration* **332**(25): 6847-6870.
[30] Sinou J-J., Lees A.W., 2005, The influence of cracks in rotating shafts, *Journal of Sound and Vibration* **285**(4-5): 1015-1037.
[31] AL-Shudeifat M.A., Butcher E.A., 2011, New breathing functions for the transverse breathing crack of the cracked rotor system: approach for critical and subcritical harmonic analysis, *Journal of Sound and Vibration* **330**(3): 526-544.
[32] Guo C., AL-Shudeifat M.A., Yan J., Bergman L.A., McFarland D.M., Butcher E.A., 2013, Stability analysis for transverse breathing cracks in rotor systems, *European Journal of Mechanics and Solids* **42**: 27-34.
[33] Pilkey W.D., 2002, *Analysis and Design of Elastic Beams*, John Wiley and Sons, New York.
[34] Bardell N.S., 1996, An engineering application of the h-p version of the finite element method to the static analysis of a Euler-Bernoulli beam, *Computers & Structures* **59**(2): 195-211.